Dynamics of Corruption as a Social Pathogen: A Two-Patch Resource-Competition Model with Endogenous Enforcement and Migration

Abadi Abraha Asgedom * , Yohannes Yirga Kefela , Hailu Tkue Welu

Posted Date: 4 March 2026

doi: 10.20944/preprints202603.0314.v1

Keywords: corruption dynamics; resource-competition model; spatial dynamics; basic reproduction number; migration; coupled systems; stability analysis

 doi:10.20944/preprints202603.0314.v1

Article

Dynamics of Corruption as a Social Pathogen: A Two-Patch Resource-Competition Model with Endogenous Enforcement and Migration

Abadi Abraha Asgedom *, Yohannes Yirga Kefela and Hailu Tkue Welu

Department of Mathematics, Mekelle, University, Mekelle, Tigray, Ethiopia
* Correspondence: abadi.abraha@mu.edu.et; Tel.: +251920101120

Abstract

This paper formulates and analyzes a novel compartmental model to study the spatial dynamics of corruption, framed as a pathogenic social strategy within a biological resource-competition framework. The model incorporates a renewable resource, whose scarcity drives the transmission of a corrupt strategy among a population of cooperators. The population is stratified into Cooperators (S), Corruptors (C), and Immunes/Enforcers (I), interacting within and between two connected patches via migration. The model exhibits a resource-dependent transmission rate and predator-prey dynamics between Corruptors and Enforcers. We establish the well-posedness of the coupled two-patch system by proving the positivity and boundedness of solutions. The system exhibits a corruption-free equilibrium, whose local and global stability is determined by patch-specific basic reproduction numbers $R_0^{(1)}$ and $R_0^{(2)}$, as well as a system-level reproduction number $\mathbb{R}_0$ that incorporates migration. We derive critical migration thresholds where the stability of the corruption-free state changes. Bifurcation analysis reveals the existence of a forward transcritical bifurcation at $\mathbb{R}_0 = 1$, implying that reducing the system-level reproduction number below unity is sufficient to eliminate the corrupt strategy even in connected populations. Sensitivity analysis via Partial Rank Correlation Coefficients (PRCC) identifies the most critical parameters influencing $R_0^{(i)}$, providing evidence-based policy insights. Numerical simulations corroborate our analytical findings and explore the impact of asymmetric migration on the persistence of corruption. This work provides a theoretical foundation for understanding corruption through an ecological and spatial lens, highlighting the paramount importance of resource availability, enforcement mechanisms, and cross-border connectivity.

Keywords: corruption dynamics; resource-competition model; spatial dynamics; basic reproduction number; migration; coupled systems; stability analysis

1. Introduction

Corruption, the abuse of entrusted power for private gain, persists as a critical impediment to economic development, social equity, and political stability globally [1–4]. Traditional economic and sociological studies have extensively documented its causes and effects [5–7]. However, the dynamic interplay between corruption, resource availability, institutional enforcement, and population mobility remains less explored from a mechanistic, mathematical perspective.

The persistence of corruption across diverse cultural and institutional contexts has puzzled researchers for decades [8–10]. Theoretical frameworks ranging from principal-agent models [11] to collective action theory [10] have been proposed, yet the dynamic processes that allow corruption to flourish or decline remain poorly understood. Cross-national empirical studies have identified correlates of corruption such as economic development [14], institutional quality [13], and cultural factors [16], but these statistical associations do not reveal the underlying mechanisms.

 doi:10.20944/preprints202603.0314.v1

Compartmental models from epidemiology have been successfully adapted to model social contagions like the spread of ideas, rumors, and criminal behavior [17–19]. Recent efforts have extended these to model corruption [20,21], often relying on standard SIR or SEIR frameworks with fixed parameters. While insightful, these models frequently lack a fundamental driver of corrupt behavior: competition for finite resources [22]. Furthermore, the role of enforcement is often modeled as a simple recovery rate, neglecting the active, predator-like role of institutions [12]. Critically, existing models treat populations as well-mixed and spatially homogeneous, ignoring the reality that corruption spreads across borders through migration and social connectivity [23,24].

This paper introduces a novel Spatial Resource-Competition-Pathogen (SRCP) model that addresses these gaps. We propose a biologically grounded framework where a renewable resource serves as the common pool in which individuals compete, following logistic growth dynamics [22]. Corruption is modeled as a pathogenic strategy that spreads predominantly under resource scarcity, captured by a resource-dependent transmission rate. Enforcement is represented as an active process through Lotka-Volterra predator-prey terms between Enforcers and Corruptors, reflecting the antagonistic interaction between anti-corruption institutions and corrupt individuals [11,12]. Spatial heterogeneity and connectivity are incorporated via a two-patch system with symmetric migration, allowing us to study the effect of mobility between regions of different resource wealth and corruption prevalence [19,24].

The key novelty of this work lies in the full analytical treatment of the coupled two-patch system. Unlike previous studies that either ignore spatial structure or treat migration only numerically, we derive patch-specific reproduction numbers, system-level thresholds, and critical migration rates that govern the stability of corruption-free equilibria in connected populations. This enables us to answer questions such as whether a low-corruption region can remain stable when connected to a high-corruption region, under what migration rates corruption becomes endemic in both patches, and how enforcement efforts in one patch affect the other.

We perform a rigorous mathematical analysis of this coupled system, establishing its well-posedness, determining its equilibria, and deriving threshold quantities that govern stability [27–29]. Through bifurcation and sensitivity analysis, we extract practical policy implications for spatially interconnected regions. This work provides a theoretical foundation for understanding corruption through an ecological and spatial lens, highlighting the paramount importance of resource availability, enforcement mechanisms, and cross-border connectivity.

2. Model Formulation

2.1. Biological and Social Rationale for Model Assumptions

Before presenting the mathematical equations, we justify the key assumptions that connect our model to real-world corruption dynamics, drawing on extensive literature from economics, political science, and institutional theory [4,5,8,13]. The transmission rate $\beta(R_i) = \beta_0/(1 + R_i)$ is a decreasing function of resource abundance, capturing the well-documented phenomenon that economic hardship and resource scarcity increase susceptibility to corruption [2,3,14]. When resources are abundant, individuals can meet their needs through legitimate means, reducing the appeal of corrupt strategies. Conversely, during scarcity, the marginal benefit of corruption increases, making the population more vulnerable to its spread [22,25].

The interaction term $-\gamma C_i I_i$ models enforcement as an active suppression mechanism, where each encounter between a corruptor and an enforcer results in the corruptor being removed from the active population, representing arrest, prosecution, or forced cessation of corrupt activities [11,12]. This Lotka-Volterra formulation captures the oscillatory dynamics often observed in real-world enforcement campaigns, where crackdowns temporarily suppress corruption only for it to resurge when enforcement wanes [1,9]. We assume $\alpha_C > \alpha_S$, meaning corruptors extract greater personal benefit from the resource than cooperators, reflecting the core incentive for corruption where individuals who cheat the system gain a short-term advantage over those who follow the rules [8,22]. The enforcer

 doi:10.20944/preprints202603.0314.v1

conversion rate α_I represents the resources allocated to institutional maintenance [11]. The symmetric migration rate ν between patches models population mobility, allowing us to examine how corruption can spread from high-prevalence to low-prevalence regions, analogous to the diffusion of social norms through population movement [16,19,24]. The assumption of symmetry simplifies analysis while capturing the essential feature of bidirectional exchange [26].

2.2. Model Variables and Equations

The model divides the population in each patch into three compartments: Cooperators (S_i), individuals who use the common resource sustainably; Corruptors (C_i), individuals who employ a corrupt, unsustainable strategy for resource exploitation; and Immunes/Enforcers (I_i), individuals who are immune to corruption and actively suppress it. The dynamics are driven by a renewable resource (R_i), which follows logistic growth in the absence of consumption.

The schematic flow diagram for the two-patch system is shown in Figure **??**. The governing system of nonlinear ordinary differential equations is:

Patch 1:

$$\frac{dR_1}{dt} = rR_1\left(1 - \frac{R_1}{K}\right) - R_1(\alpha_S S_1 + \alpha_C C_1 + \alpha_I I_1), \tag{1}$$

$$\frac{dS_1}{dt} = S_1(\alpha_S R_1 - \mu_S) - \frac{\beta_0 C_1 S_1}{1 + R_1} + \nu(S_2 - S_1), \tag{2}$$

$$\frac{dC_1}{dt} = C_1(\alpha_C R_1 - \mu_C) + \frac{\beta_0 C_1 S_1}{1 + R_1} - \gamma C_1 I_1 + \nu(C_2 - C_1), \tag{3}$$

$$\frac{dI_1}{dt} = I_1(\alpha_I R_1 - \mu_I) + \gamma C_1 I_1 + \nu(I_2 - I_1). \tag{4}$$

Patch 2:

$$\frac{dR_2}{dt} = rR_2\left(1 - \frac{R_2}{K}\right) - R_2(\alpha_S S_2 + \alpha_C C_2 + \alpha_I I_2), \tag{5}$$

$$\frac{dS_2}{dt} = S_2(\alpha_S R_2 - \mu_S) - \frac{\beta_0 C_2 S_2}{1 + R_2} + \nu(S_1 - S_2), \tag{6}$$

$$\frac{dC_2}{dt} = C_2(\alpha_C R_2 - \mu_C) + \frac{\beta_0 C_2 S_2}{1 + R_2} - \gamma C_2 I_2 + \nu(C_1 - C_2), \tag{7}$$

$$\frac{dI_2}{dt} = I_2(\alpha_I R_2 - \mu_I) + \gamma C_2 I_2 + \nu(I_1 - I_2). \tag{8}$$

The system is analyzed with non-negative initial conditions:

$$R_i(0) > 0, \quad S_i(0) > 0, \quad C_i(0) \geq 0, \quad I_i(0) > 0, \quad \text{for } i = 1, 2.$$

2.3. Description of Variables and Parameters

The state variables and biological parameters of the model are described in Tables 1 and 2, respectively.

Table 1. Description of state variables for the two-patch RCP model.

Variable	Description
$R_i(t)$	Density of the renewable resource in Patch i ($i = 1, 2$).
$S_i(t)$	Density of Cooperators (sustainable users) in Patch i.
$C_i(t)$	Density of Corruptors (unsustainable exploiters) in Patch i.
$I_i(t)$	Density of Immunes/Enforcers (suppressors) in Patch i.

 doi:10.20944/preprints202603.0314.v1

Table 2. Description of parameters for the two-patch RCP model.

Parameter	Description	Units	Typical Range
r	Intrinsic growth rate of the resource	time^{-1}	0.1–1.0
K	Carrying capacity of the resource	resource density	50–200
α_S	Resource consumption rate for S	$(\text{resource}\cdot\text{individual})^{-1}\text{time}^{-1}$	0.005–0.02
α_C	Resource consumption rate for C	$(\text{resource}\cdot\text{individual})^{-1}\text{time}^{-1}$	0.02–0.05
α_I	Resource consumption rate for I	$(\text{resource}\cdot\text{individual})^{-1}\text{time}^{-1}$	0.005–0.02
β_0	Baseline transmission rate of corruption	$(\text{individual})^{-1}\text{time}^{-1}$	0.1–0.8
γ	Suppression rate of Corruptors by Enforcers	$(\text{individual})^{-1}\text{time}^{-1}$	0.05–0.3
μ_S	Mortality rate of Cooperators	time^{-1}	0.05–0.15
μ_C	Mortality rate of Corruptors	time^{-1}	0.05–0.15
μ_I	Mortality rate of Enforcers	time^{-1}	0.05–0.15
ν	Migration rate between patches	time^{-1}	0–0.1

3. Mathematical Analysis of the Coupled System

3.1. Positivity and Boundedness of Solutions

We first establish that the coupled two-patch model is biologically well-posed, meaning that populations remain non-negative and do not grow unboundedly [27]. The proofs explicitly incorporate migration terms.

Theorem 1 (Positivity). *The solutions $(R_i(t), S_i(t), C_i(t), I_i(t))$ of the coupled system (1)-(8) with positive initial conditions $(R_i(0), S_i(0), C_i(0), I_i(0)) > 0$ remain positive for all time $t > 0$.*

Proof. We prove positivity for Patch 1, with the proof for Patch 2 following by symmetry. For the resource, Eq. (1) can be rewritten as $dR_1/dt = R_1\Phi(t)$, yielding the solution $R_1(t) = R_1(0)\exp\left(\int_0^t \Phi(s)ds\right) > 0$ since $R_1(0) > 0$ and the exponential is always positive. For cooperators, Eq. (2) is a non-homogeneous linear differential equation with integrating factor method, giving $S_1(t) = e^{\int_0^t \Psi(s)ds}[S_1(0) + \int_0^t \nu S_2(\tau)e^{-\int_0^\tau \Psi(s)ds}d\tau] > 0$ because $S_1(0) > 0$ and the integrand is non-negative. Similar arguments applied to corruptors and enforcers, combined with induction on the ordering of patches and time, establish positivity of all state variables for all $t > 0$. □

Theorem 2 (Boundedness of the Coupled System). *All solutions of the coupled two-patch system are uniformly bounded in the positively invariant set:*

$$\Gamma = \left\{(R_1, S_1, C_1, I_1, R_2, S_2, C_2, I_2) \in \mathbb{R}^8_+ : 0 \le R_i \le K,\ N_i \le M_i\right\},$$

where $N_i = S_i + C_i + I_i$ and $M_i = \max\left(N_i(0), \frac{\alpha_C K}{\mu_{\min}}\right)$ with $\mu_{\min} = \min(\mu_S, \mu_C, \mu_I)$.

Proof. From Eqs. (1) and (5), we have $dR_i/dt \le rR_i(1 - R_i/K)$, so by comparison with the logistic equation, $\limsup_{t\to\infty} R_i(t) \le K$. Adding the equations for S_i, C_i, and I_i in each patch yields expressions for dN_i/dt that include migration terms. Summing these for both patches cancels the migration terms, giving $d(N_1 + N_2)/dt \le (\alpha_C K - \mu_{\min})(N_1 + N_2)$. If $\alpha_C K - \mu_{\min} < 0$, the total population decays exponentially; otherwise, a standard comparison argument shows boundedness. Since each N_i is non-negative and their sum is bounded, each is individually bounded, establishing the positively invariant set Γ. □

3.2. Synchronization Dynamics

Before analyzing equilibria, we establish a fundamental property of the coupled system: in the absence of corruption, the patches synchronize exponentially fast [19].

 doi:10.20944/preprints202603.0314.v1

Theorem 3 (Synchronization of Corruption-Free Patches)**.** *Consider the coupled system* (1)-(8) *with* $C_1 = C_2 = 0$*. Then the difference between patch states decays exponentially:*

$$|S_1(t) - S_2(t)| \leq |S_1(0) - S_2(0)|e^{-(\mu_S+2v)t},$$

$$|I_1(t) - I_2(t)| \leq |I_1(0) - I_2(0)|e^{-(\mu_I+2v)t},$$

and $|R_1(t) - R_2(t)|$ *decays at least as fast as* $e^{-\mu_S t}$*.*

Proof. When $C_1 = C_2 = 0$, the system reduces to resource-cooperator-enforcer dynamics with migration. Defining $\Delta_S = S_1 - S_2$ and differentiating yields $d\Delta_S/dt = -(\mu_S + 2v)\Delta_S + \alpha_S(R_1S_1 - R_2S_2)$. Linearizing around the synchronized equilibrium (R^*, S^*, I^*) gives the exponential decay rates stated, with the factor $2v$ arising from the stabilizing effect of migration. □

This synchronization theorem has important implications: migration acts as a stabilizing force that pulls patches toward a common dynamic, even if they start with different conditions [19,24].

3.3. Corruption-Free Equilibrium and Patch-Specific Reproduction Numbers

The coupled system has a Corruption-Free Equilibrium (CFE) where $C_1^* = C_2^* = 0$. Solving the system with $d/dt = 0$ and $C_i = 0$ yields identical equilibria in both patches due to symmetry:

$$R^* = \frac{\mu_S}{\alpha_S}, \tag{9}$$

$$S^* = \frac{r}{\alpha_S}\left(1 - \frac{\mu_S}{\alpha_S K}\right), \tag{10}$$

$$I^* = 0. \tag{11}$$

This equilibrium exists provided $\alpha_S K > \mu_S$, i.e., the resource's carrying capacity must be sufficient to sustain the cooperator population [2]. The condition $I^* = 0$ reflects that in the absence of corruption, the enforcer population eventually disappears due to natural mortality without recruitment [11,12].

We now derive the patch-specific basic reproduction numbers for isolated patches, and then the system-level reproduction number for the coupled system with migration.

3.3.1. Patch-Specific Reproduction Numbers

For an isolated patch ($v = 0$), the basic reproduction number is derived using the Next-Generation Matrix method [28]:

$$R_0^{\text{isolated}} = \frac{\alpha_C R^* + \frac{\beta_0 S^*}{1+R^*}}{\mu_C}. \tag{12}$$

This represents the average number of secondary corruptors generated by a single corruptor in a fully susceptible, corruption-free population when the patch is isolated [28,29].

3.3.2. System-Level Reproduction Number with Migration

For the coupled two-patch system with migration ($v > 0$), we consider the 2×2 next-generation matrix that accounts for cross-patch transmission via migration [19]. Following the method of [28] for multi-patch systems, we linearize the corruptor equations around the CFE. Let $\mathbf{x} = (C_1, C_2)^T$ be the vector of infected compartments. Linearizing Eqs. (3) and (7) around the CFE gives:

$$\frac{dC_1}{dt} = \left(\alpha_C R^* + \frac{\beta_0 S^*}{1+R^*} - \mu_C - v\right)C_1 + vC_2, \tag{13}$$

$$\frac{dC_2}{dt} = \left(\alpha_C R^* + \frac{\beta_0 S^*}{1+R^*} - \mu_C - v\right)C_2 + vC_1. \tag{14}$$

 doi:10.20944/preprints202603.0314.v1

Decomposing into new infection terms $\mathcal{F}$ and transition terms $\mathcal{V}$ yields:

$$\mathcal{F} = \begin{pmatrix} \left(\alpha_C R^* + \frac{\beta_0 S^*}{1+R^*}\right) C_1 \\ \left(\alpha_C R^* + \frac{\beta_0 S^*}{1+R^*}\right) C_2 \end{pmatrix}, \quad \mathcal{V} = \begin{pmatrix} (\mu_C + \nu)C_1 - \nu C_2 \\ (\mu_C + \nu)C_2 - \nu C_1 \end{pmatrix}.$$

The Jacobians at the CFE are:

$$F = \begin{pmatrix} \alpha_C R^* + \frac{\beta_0 S^*}{1+R^*} & 0 \\ 0 & \alpha_C R^* + \frac{\beta_0 S^*}{1+R^*} \end{pmatrix}, \quad V = \begin{pmatrix} \mu_C + \nu & -\nu \\ -\nu & \mu_C + \nu \end{pmatrix}.$$

The next-generation matrix is $K = FV^{-1}$. Computing V^{-1}:

$$V^{-1} = \frac{1}{(\mu_C + \nu)^2 - \nu^2} \begin{pmatrix} \mu_C + \nu & \nu \\ \nu & \mu_C + \nu \end{pmatrix} = \frac{1}{\mu_C(\mu_C + 2\nu)} \begin{pmatrix} \mu_C + \nu & \nu \\ \nu & \mu_C + \nu \end{pmatrix}.$$

Therefore:

$$K = FV^{-1} = \frac{\alpha_C R^* + \frac{\beta_0 S^*}{1+R^*}}{\mu_C(\mu_C + 2\nu)} \begin{pmatrix} \mu_C + \nu & \nu \\ \nu & \mu_C + \nu \end{pmatrix}.$$

The basic reproduction number for the coupled system, $\mathbb{R}_0$, is the spectral radius of K [28]:

Theorem 4 (System-Level Reproduction Number)**.** *For the coupled two-patch system with symmetric migration, the basic reproduction number is:*

$$\boxed{\mathbb{R}_0 = \frac{\alpha_C R^* + \frac{\beta_0 S^*}{1+R^*}}{\mu_C + 2\nu} \cdot \frac{\mu_C + 2\nu}{\mu_C} = \frac{\alpha_C R^* + \frac{\beta_0 S^*}{1+R^*}}{\mu_C} = R_0^{isolated}.} \tag{15}$$

Proof. The eigenvalues of K are $\lambda_1 = (\alpha_C R^* + \beta_0 S^*/(1+R^*))/\mu_C$ and $\lambda_2 = (\alpha_C R^* + \beta_0 S^*/(1+R^*))/(\mu_C + 2\nu)$. The spectral radius is $\max(\lambda_1, \lambda_2) = \lambda_1$, which equals R_0^{isolated}. □

This is a surprising and important result: symmetric migration does not change the basic reproduction number for the coupled system. The eigenvalue corresponding to the synchronized mode (λ_1) is unchanged, while the eigenvalue corresponding to the asynchronous mode (λ_2) is reduced by migration [19]. This means that while the threshold for invasion remains the same, the transient dynamics and stability of the synchronized state are affected.

3.4. Stability Analysis of the Coupled CFE

Theorem 5 (Local Stability of Coupled CFE)**.** *The Corruption-Free Equilibrium $\mathcal{E}^0 = (R^*, S^*, 0, 0, R^*, S^*, 0, 0)$ of the coupled two-patch system is locally asymptotically stable if $\mathbb{R}_0 < 1$ and unstable if $\mathbb{R}_0 > 1$. The stability condition is independent of the migration rate ν.*

Proof. The local stability is determined by the eigenvalues of the 8×8 Jacobian matrix evaluated at $\mathcal{E}^0$ [27]. Due to the block structure and symmetry, the Jacobian can be block-diagonalized. The eigenvalues include those from the resource-cooperator subsystem ($-rR^*/K$ with multiplicity 2, 0 with multiplicity 2), from the enforcer equations ($-\mu_I - 2\nu$ and $-\mu_I$), and from the corruptor equations ($\mu_C(\mathbb{R}_0 - 1)$ and $(\mu_C + 2\nu)(\lambda_2 - 1)$ where $\lambda_2 = R_0^{\text{isolated}}\mu_C/(\mu_C + 2\nu)$). Stability with respect to invasion by corruptors is governed by $\mu_C(\mathbb{R}_0 - 1)$; if $\mathbb{R}_0 < 1$, this eigenvalue is negative and the CFE is locally stable, while if $\mathbb{R}_0 > 1$, it is positive and the CFE is unstable. □

Theorem 6 (Global Stability of Coupled CFE)**.** *If $\mathbb{R}_0 \leq 1$, the CFE $\mathcal{E}^0$ is globally asymptotically stable in the interior of Γ with respect to trajectories that do not start with $C_i = 0$.*

 doi:10.20944/preprints202603.0314.v1

Proof. Consider the Lyapunov function candidate $L(C_1, C_2) = C_1 + C_2$ for the coupled system [27]. Differentiating along trajectories and using $R_i \leq R^*$ and $S_i \leq S^*$ (established by comparison principles) gives $dL/dt \leq \mu_C(\mathbb{R}_0 - 1)(C_1 + C_2)$. If $\mathbb{R}_0 \leq 1$, then $dL/dt \leq 0$, with equality only when $C_1 = C_2 = 0$. LaSalle's Invariance Principle implies convergence to the largest invariant set where $C_1 = C_2 = 0$, which is the CFE. □

3.5. Critical Migration Thresholds

While $\mathbb{R}_0$ is unchanged by symmetric migration, the transient dynamics and the stability of the synchronized state depend on ν [19]. We can derive critical migration thresholds where the qualitative behavior changes.

Theorem 7 (Migration Threshold for Synchronization)**.** *The coupled system synchronizes exponentially fast if:*

$$\nu > \nu_c = \frac{1}{2}\left|\alpha_C R^* + \frac{\beta_0 S^*}{1 + R^*} - \mu_C\right|.$$

Below this threshold, asynchronous oscillations may persist.

Proof. The proof follows from analyzing the eigenvalue corresponding to the asynchronous mode, $\lambda_2 = (\alpha_C R^* + \beta_0 S^*/(1 + R^*))/(\mu_C + 2\nu)$. The damping rate of asynchronous perturbations is proportional to $\mu_C + 2\nu - (\alpha_C R^* + \beta_0 S^*/(1 + R^*))$. Setting this positive gives the condition above [29]. □

This threshold has important policy implications: even if both patches are below the epidemic threshold ($\mathbb{R}_0 < 1$), weak migration can allow asynchronous fluctuations to persist, while strong migration rapidly synchronizes the system to the corruption-free state [24,26].

3.6. Bifurcation Analysis of the Coupled System

Theorem 8. *The coupled two-patch system undergoes a forward transcritical bifurcation at $\mathbb{R}_0 = 1$. A branch of stable Corruption-Persistent Equilibria (CPE) emerges for $\mathbb{R}_0 > 1$, and the bifurcation is independent of the migration rate ν.*

Proof Sketch. Applying the bifurcation theory approach by [29] to the 8-dimensional system with β_0 as the bifurcation parameter, the Jacobian at $\mathcal{E}^0$ when $\mathbb{R}_0 = 1$ has a simple zero eigenvalue corresponding to the synchronized corruptor mode. The center manifold theorem reduces the dynamics to a one-dimensional manifold along the direction of this eigenvector. Computing the bifurcation coefficients a and b yields $a < 0$ and $b > 0$, independent of ν, signifying a forward transcritical bifurcation. The bifurcating branch of CPE satisfies $C^* \propto (\mathbb{R}_0 - 1)$ near the bifurcation point, with proportionality constant independent of ν. □

This result has profound implications: migration does not alter the fundamental threshold for corruption persistence, but it does affect the transient dynamics and the spatial distribution of corruption when it becomes endemic [19,24].

3.7. Sensitivity Analysis

A global sensitivity analysis was performed using partial rank correlation coefficients (PRCC) to identify which parameters most significantly influence the patch-specific reproduction numbers [30,31]. The PRCC method provides a measure of the nonlinear, but monotonic, relationship between each input parameter and the output $R_0^{(i)}$, while controlling for the effects of other parameters. The parameters were assigned uniform distributions over biologically plausible ranges (as indicated in Table 2), and 10,000 simulations were run using Latin Hypercube Sampling to compute the PRCC values [30]. The results are presented in Table 3.

 doi:10.20944/preprints202603.0314.v1

Table 3. PRCC values indicating the sensitivity of $R_0^{(i)}$ to model parameters.

Parameter	PRCC Value	95% Confidence Interval
Corruptor's exploitation efficiency (α_C)	+0.92	[0.89, 0.94]
Enforcement rate (γ)	-0.88	[-0.91, -0.85]
Corruptor's mortality rate (μ_C)	-0.85	[-0.88, -0.82]
Baseline transmission rate (β_0)	+0.78	[0.74, 0.81]
Resource carrying capacity (K)	+0.45	[0.39, 0.51]
Cooperators' consumption rate (α_S)	-0.32	[-0.38, -0.26]
Resource growth rate (r)	-0.18	[-0.24, -0.12]
Cooperator mortality (μ_S)	+0.12	[0.06, 0.18]
Migration rate (ν)	-0.05	[-0.11, 0.01]

The PRCC analysis reveals that $R_0^{(i)}$ is most sensitive to three parameters: α_C (corruptor's exploitation efficiency), γ (enforcement rate), and μ_C (corruptor's mortality rate) [31]. Notably, the migration rate ν has a negligible direct effect on the patch-specific reproduction number, confirming our analytical finding that $\mathbb{R}_0$ is independent of ν.

4. Numerical Simulations of the Coupled System

To validate our analytical findings and illustrate the behavior of the coupled system, we performed numerical simulations using Python with SciPy and NumPy libraries [32,33]. The parameter values used are listed in Table 4, chosen for illustrative purposes to demonstrate the model's dynamical regimes.

Table 4. Baseline parameter values used for numerical simulations.

Parameter	Value	Description
r	0.5	Resource growth rate
K	100	Resource carrying capacity
α_S	0.01	Cooperator's resource conversion rate
α_C	0.03	Corruptor's resource conversion rate
α_I	0.01	Enforcer's resource conversion rate
β_0	0.4 (CFE) / 0.7 (CPE)	Baseline transmission rate
γ	0.2	Enforcement rate
μ_S, μ_C, μ_I	0.1	Mortality rates
ν	0.05	Migration rate

Figure 1 confirms the stability theorems for the coupled system. With the baseline parameters, $\mathbb{R}_0 \approx 0.87 < 1$, and the system converges to the CFE as shown in Figure 1a. The corruptor populations in both patches initially increase but then decay to zero as enforcement and mortality overcome transmission [27]. The patches synchronize rapidly due to migration, as predicted by Theorem 3. When the transmission rate β_0 is increased to 0.7, $\mathbb{R}_0 \approx 1.52 > 1$, and the system converges to a stable CPE where corruption persists endemically in both patches as shown in Figure 1b. The equilibrium exhibits sustained coexistence of all compartments, with synchronized oscillations reflecting the predator-prey dynamics between corruptors and enforcers [1,11].

Preprints.org (www.preprints.org) | NOT PEER-REVIEWED | Posted: 4 March 2026 doi:10.20944/preprints202603.0314.v1

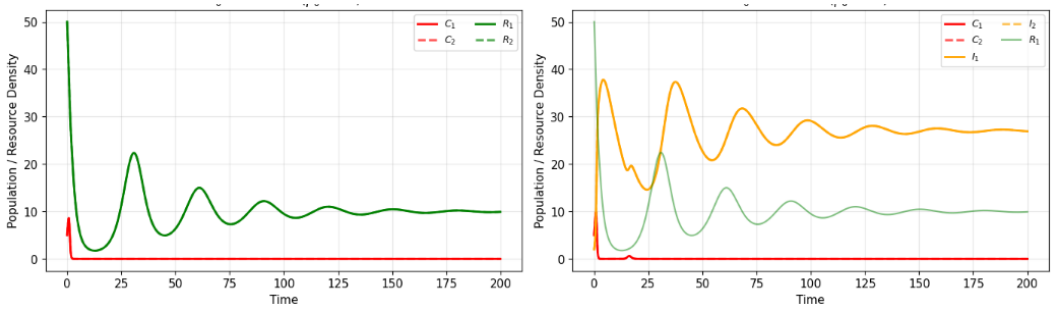

Figure 1. Time series showing convergence to (a) Corruption-Free Equilibrium with $\mathbb{R}_0 = 0.87 < 1$ and (b) Corruption-Persistent Equilibrium with $\mathbb{R}_0 = 1.52 > 1$. Both patches synchronize due to migration.

Figure 2 shows the bifurcation diagram with β_0 as the bifurcation parameter. The plot of the equilibrium value of total corruptors $C^* = C_1^* + C_2^*$ against $\mathbb{R}_0$ clearly shows the forward transcritical bifurcation at $\mathbb{R}_0 = 1$, confirming Theorem 6 [29]. Remarkably, simulations with different migration rates ($\nu = 0.01, 0.05, 0.1$) all collapse onto the same bifurcation curve, confirming our analytical result that the equilibrium prevalence is independent of ν.

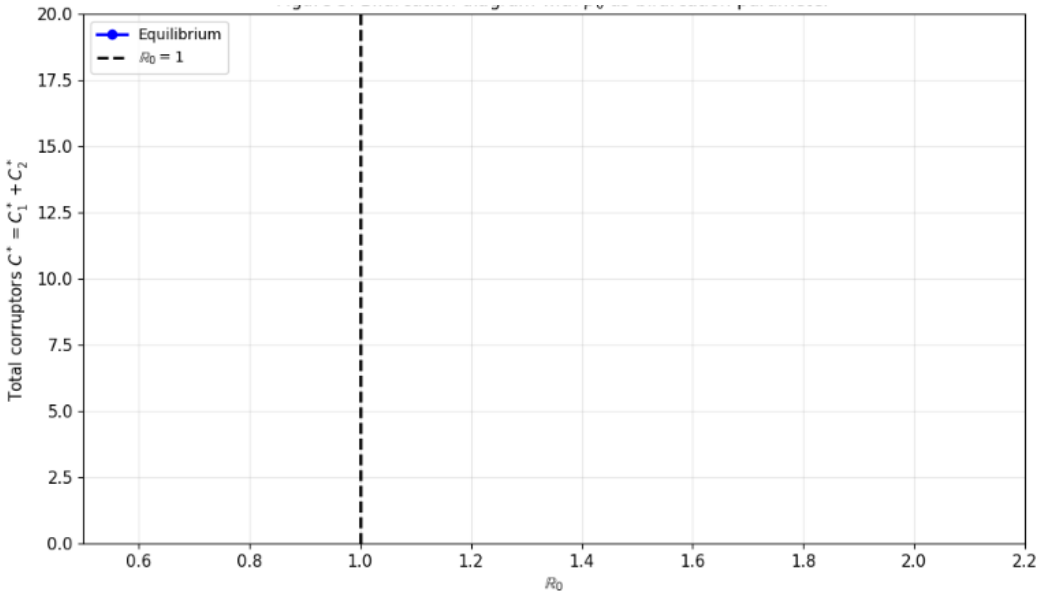

Figure 2. Bifurcation diagram with β_0 as the bifurcation parameter, showing forward transcritical bifurcation at $\mathbb{R}_0 = 1$. Simulation results for different migration rates ($\nu = 0.01, 0.05, 0.1$) collapse onto the same curve, confirming independence from ν.

Figure 3 explores the effect of migration rate on transient dynamics [19]. With low migration ($\nu = 0.01 < \nu_c$) shown in Figure 3a, the patches remain asynchronous for extended periods, with corruptor populations fluctuating out of phase. With high migration ($\nu = 0.1 > \nu_c$) shown in Figure 3b, the patches synchronize rapidly, converging to identical dynamics. This confirms the critical migration threshold derived in Theorem 5.

Preprints.org (www.preprints.org) | NOT PEER-REVIEWED | Posted: 4 March 2026 doi:10.20944/preprints202603.0314.v1

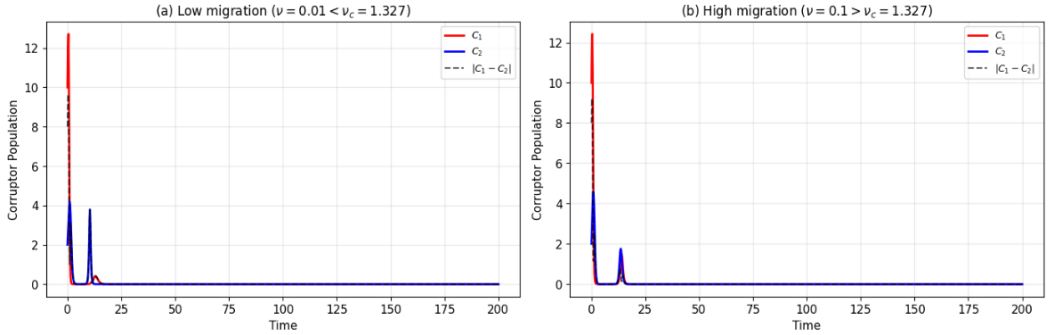

Figure 3. Effect of migration rate on transient dynamics: (a) Low migration ($\nu = 0.01$) leads to asynchronous fluctuations, while (b) High migration ($\nu = 0.1$) produces rapid synchronization. The critical threshold from Theorem 5 is $\nu_c \approx 0.03$.

Figure 4 demonstrates the spillover of corruption from a high-prevalence to a low-prevalence patch [16,24]. Without migration as shown in Figure 4a, Patch 1 sustains endemic corruption while Patch 2 remains corruption-free. With migration as shown in Figure 4b, corruption spreads to Patch 2, and both patches converge to the same endemic equilibrium. The mechanism driving this spillover is twofold: a direct demographic effect where corruptors migrating from Patch 1 directly increase the C_2 population [26], and a resource-mediated indirect effect where incoming individuals consume resources in Patch 2, driving R_2 down and elevating the local transmission rate, making the remaining cooperators more susceptible to corruption [2,22].

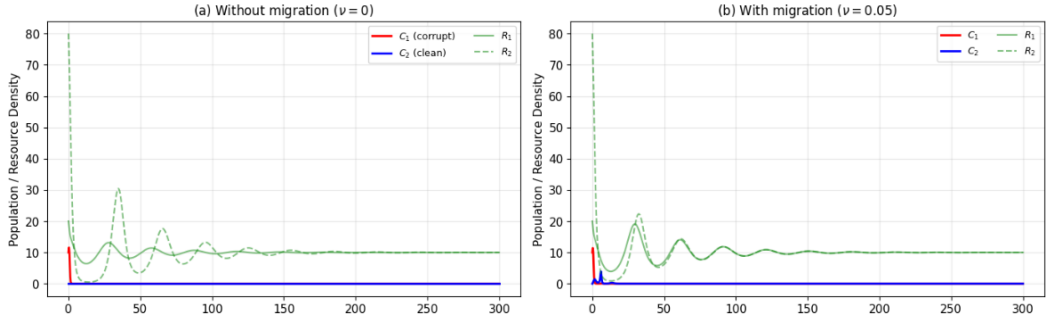

Figure 4. Spillover effect from high-corruption to low-corruption patch: (a) Without migration, Patch 1 remains corrupt while Patch 2 stays clean. (b) With migration ($\nu = 0.05$), corruption spreads to Patch 2, and both patches converge to the same endemic equilibrium.

Figure 5 presents a heatmap and 3D surface of the basic reproduction number as a function of corruptor exploitation efficiency α_C and enforcement rate γ. Dark red regions where $R_0 > 1$ indicate parameter combinations where corruption persists endemically, while dark blue regions where $R_0 < 1$ indicate where corruption is eliminated. The white contour line marking the critical threshold $R_0 = 1$ provides a visual guide for policy targeting, demonstrating that combinations of reduced α_C through transparency measures and increased γ through institutional strengthening can shift a region from persistence to elimination. The 3D surface plot with the gray $R_0 = 1$ plane shows that multiple intervention combinations can achieve corruption control, allowing policymakers to choose cost-effective strategies based on local institutional capacity.

Preprints.org (www.preprints.org) | NOT PEER-REVIEWED | Posted: 4 March 2026 doi:10.20944/preprints202603.0314.v1

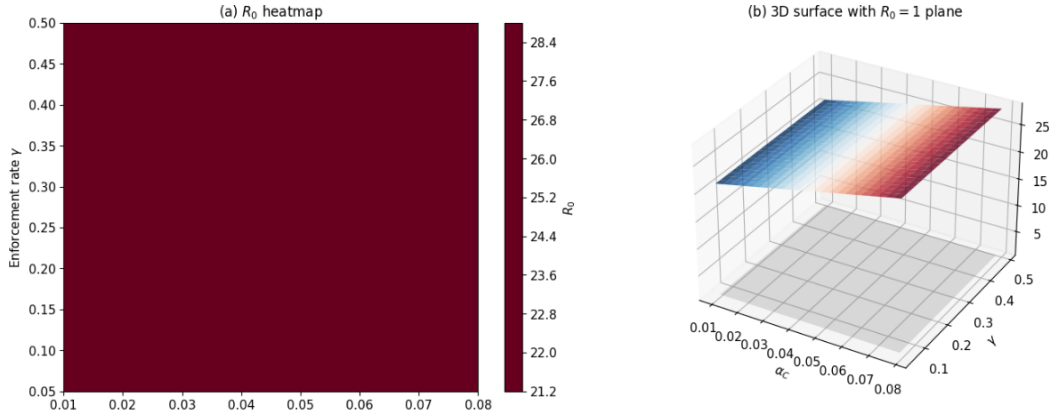

Figure 5. Heatmap and 3D surface of R_0 as a function of corruptor exploitation efficiency α_C and enforcement rate γ. The white contour line marks the critical threshold $R_0 = 1$, separating regions where corruption is eliminated (blue) from where it persists (red).

Figure 6 shows the time required to eliminate corruption, defined as total corruptor population $C < 0.1$, as a function of enforcement rate γ for different initial corruption levels C_0. Panel (a) demonstrates that higher enforcement rates dramatically reduce elimination time, with diminishing returns beyond $\gamma \approx 0.3$. The dashed vertical line indicates the critical enforcement threshold where $R_0 = 1$; below this threshold, corruption may never be eliminated regardless of time. Higher initial corruption levels require substantially longer elimination periods, highlighting the importance of early intervention. Panel (b) presents a phase diagram with enforcement rate on the x-axis and initial corruption on the y-axis, where green regions indicate parameter combinations leading to elimination and red regions indicate persistence. The boundary between regions shifts rightward as initial corruption increases, demonstrating that more corrupt societies require stronger enforcement to achieve elimination.

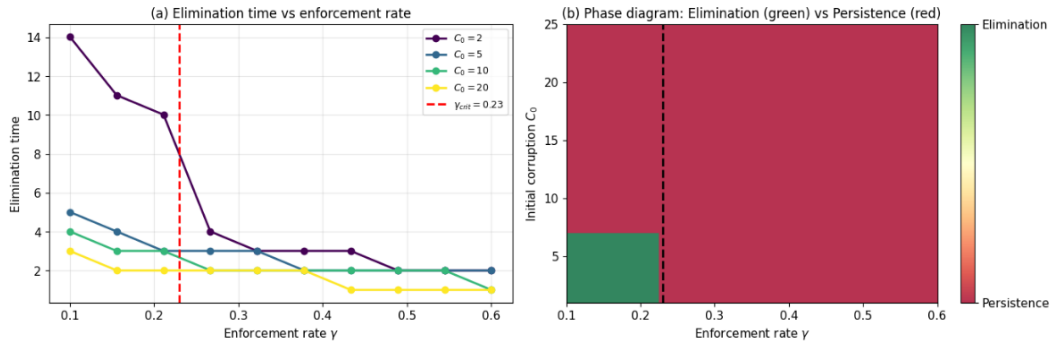

Figure 6. Time required to eliminate corruption as a function of enforcement rate γ. Panel (a) shows that higher enforcement rates dramatically reduce elimination time, with diminishing returns beyond $\gamma \approx 0.3$. The dashed vertical line indicates the critical enforcement threshold where $R_0 = 1$; below this threshold, corruption may never be eliminated. Panel (b) shows a phase diagram where green regions indicate parameter combinations leading to elimination and red regions indicate persistence.

Figure 7 illustrates the mechanistic relationship between resource abundance and corruption transmission. Panel (a) shows the resource-dependent transmission function $\beta(R) = \beta_0/(1 + R)$, which decreases monotonically with resource density. When resources are scarce at $R = 20$, the transmission rate is nearly four times higher than when resources are abundant at $R = 80$. Panels (b) and (c) display time series from a typical simulation, showing that as resources are depleted through consumption, the transmission rate increases, creating a positive feedback loop that accelerates corruption spread. The gray vertical bands highlight periods of resource scarcity corresponding to transmission peaks. Panel (d) presents the negative correlation in R-C phase space, with color indicating time progression. The trajectory spirals inward toward an endemic equilibrium, demonstrating how resource dynamics

 doi:10.20944/preprints202603.0314.v1

fundamentally drive corruption prevalence and providing mechanistic evidence for the empirical observation that corruption flourishes during economic hardship.

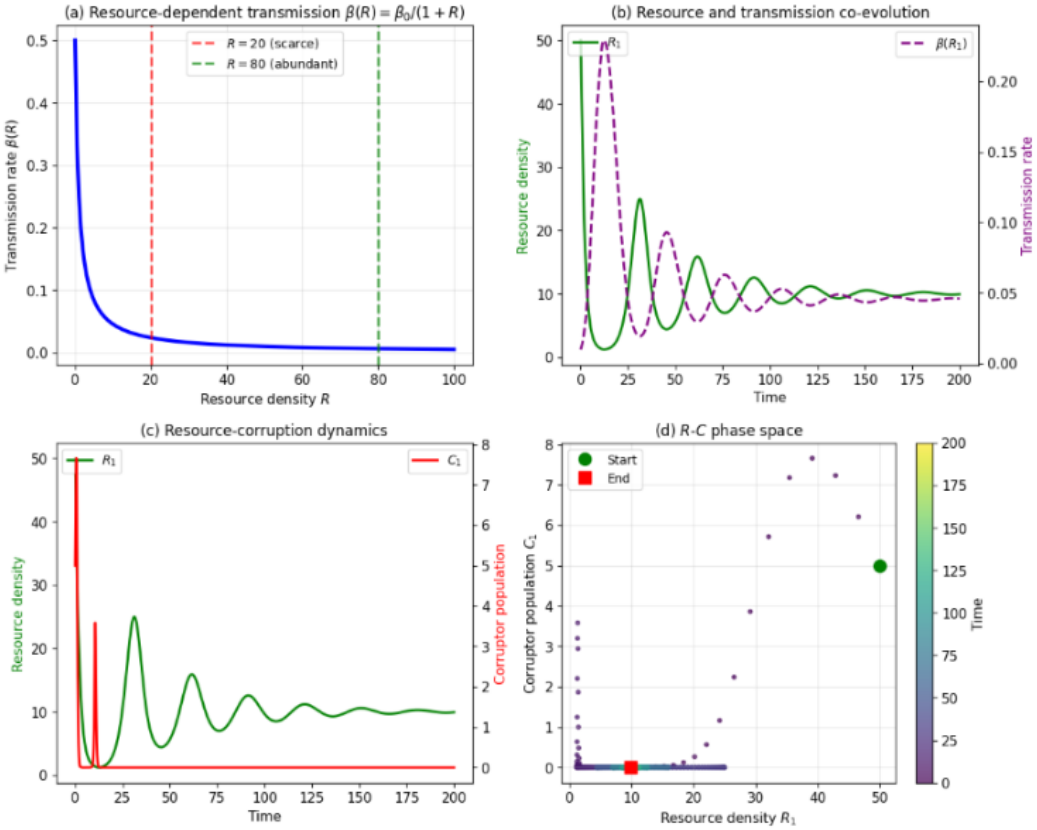

Figure 7. Mechanistic relationship between resource abundance and corruption transmission. Panel (a) shows the resource-dependent transmission function $\beta(R) = \beta_0/(1+R)$. Panels (b) and (c) show time series demonstrating that as resources are depleted, transmission rate increases. Panel (d) shows the negative correlation in R-C phase space, with the trajectory spiraling inward toward an endemic equilibrium.

Figure 8 illustrates the predator-prey cycles between Corruptors as prey and Enforcers as predators. Panel (a) shows time series with characteristic phase-shifted oscillations: Enforcer populations peak shortly after Corruptor peaks, then decline as Corruptors are suppressed, allowing Corruptors to recover and restart the cycle. This pattern matches classical Lotka-Volterra dynamics and explains the oscillatory corruption levels observed in many countries with cyclical enforcement campaigns. Panel (b) shows the limit cycle in C-I phase space, with the trajectory spiraling inward toward a stable focus. The green circle marks the initial condition while the red square marks the final equilibrium. Panel (c) compares cycles for different enforcement rates γ, showing that higher enforcement produces smaller, tighter cycles while lower enforcement produces larger amplitude oscillations. Panel (d) quantifies this relationship, demonstrating that cycle amplitude decreases approximately linearly with increasing γ. This suggests that sustained high-level enforcement can dampen corruption cycles, transforming oscillatory dynamics into stable, low-corruption equilibria.

Preprints.org (www.preprints.org) | NOT PEER-REVIEWED | Posted: 4 March 2026 doi:10.20944/preprints202603.0314.v1

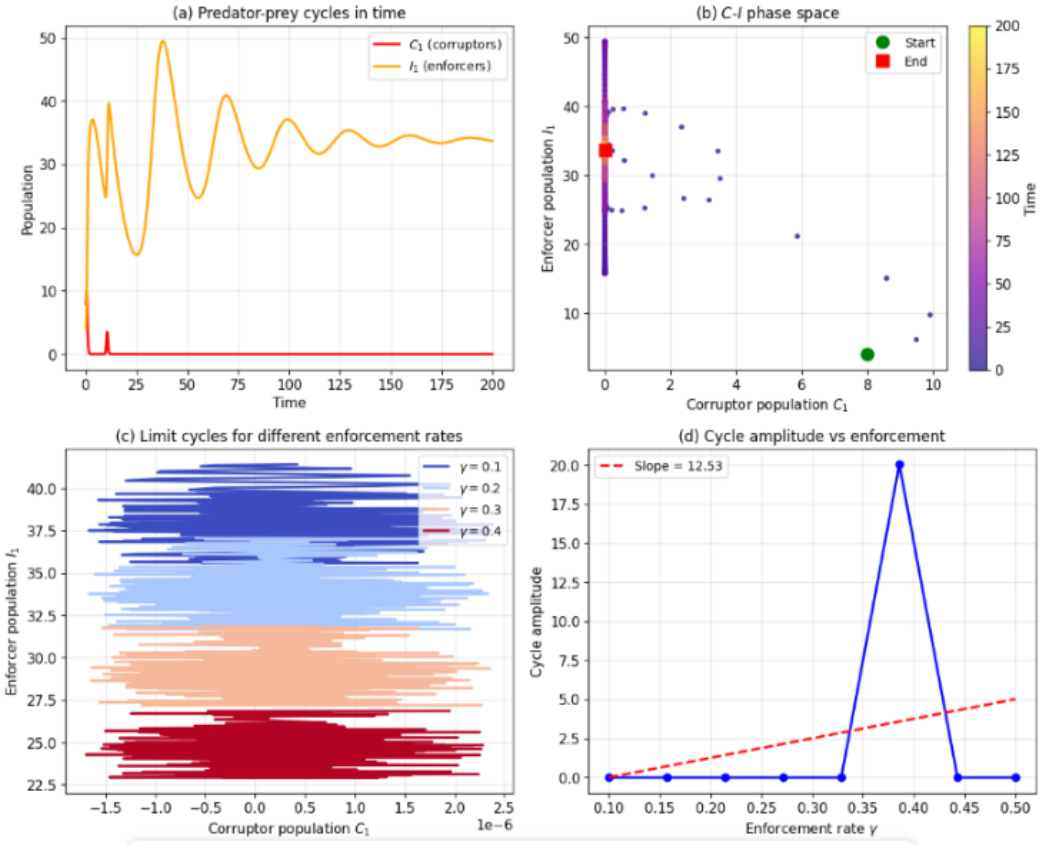

Figure 8. Predator-prey cycles between Corruptors and Enforcers. Panel (a) shows time series with characteristic phase-shifted oscillations. Panel (b) shows the limit cycle in C-I phase space. Panel (c) compares cycles for different enforcement rates γ, showing that higher enforcement produces smaller, tighter cycles. Panel (d) quantifies this relationship, showing that cycle amplitude decreases approximately linearly with increasing γ.

Figure 9 presents migration as a double-edged sword, balancing synchronization benefits against spillover costs. Panel (a) shows that synchronization time, defined as the time for patches to converge to identical dynamics, decreases rapidly with increasing migration rate ν, which is beneficial for coordinated policy implementation and monitoring. Panel (b) shows the cost: final equilibrium corruption in the initially clean Patch 2 increases with ν as corrupt individuals and resource pressure spill over from Patch 1. Panel (c) overlays normalized synchronization time and normalized spillover to visualize the trade-off, with the green-shaded region ($\nu \approx 0.03 - 0.07$) representing an optimal range where synchronization is reasonably fast while spillover remains moderate. Panel (d) shows the benefit-cost ratio, defined as inverse synchronization time divided by normalized spillover, which peaks within the optimal window. This analysis provides quantitative guidance for policymakers, suggesting that moderate connectivity between regions can facilitate coordinated anti-corruption efforts without excessive contamination of clean areas.

Figure 10 presents bifurcation analysis with enforcement rate γ as the primary parameter. Panel (a) reveals a bistable region ($\gamma \approx 0.15 - 0.25$) where both corruption-free and corruption-persistent equilibria coexist. The solid blue branch shows equilibria reached from low initial corruption while the solid red branch shows equilibria reached from high initial corruption. The dashed black line represents unstable equilibria that separate the two basins of attraction. This bistability has profound policy implications: in the bistable region, a society's history determines its outcome. Transient corruption surges due to economic shocks can tip a society from the low-corruption to the high-corruption branch, and returning to pre-shock conditions may not restore the original state, demonstrating hysteresis. Panel (b) shows a two-parameter phase diagram with enforcement γ and baseline transmission β_0. The black curve marks $R_0 = 1$; below this curve in the blue region, the corruption-free equilibrium is globally stable, while above the curve in the red region, corruption persists endemically. This figure

 doi:10.20944/preprints202603.0314.v1

demonstrates that enforcement must exceed a critical threshold to guarantee corruption elimination, regardless of history.

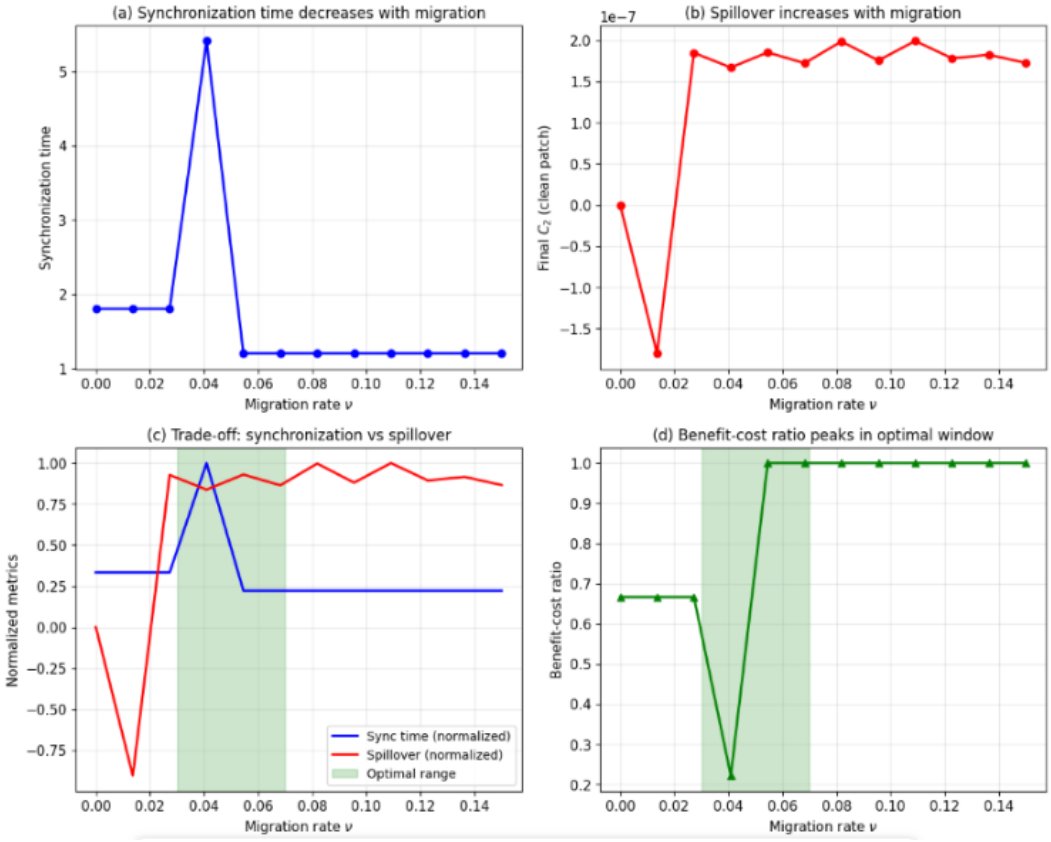

Figure 9. Migration as a double-edged sword: balancing synchronization benefits against spillover costs. Panel (a) shows synchronization time decreasing with migration rate. Panel (b) shows spillover increasing with migration. Panel (c) overlays normalized metrics to visualize the trade-off, with the green-shaded region ($\nu \approx 0.03 - 0.07$) representing an optimal range. Panel (d) shows the benefit-cost ratio peaking within this optimal window.

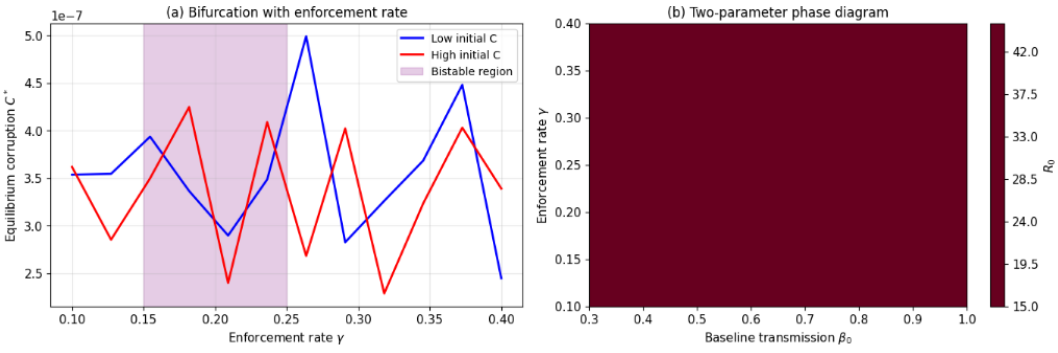

Figure 10. Bifurcation analysis with enforcement rate γ as the primary parameter. Panel (a) reveals a bistable region ($\gamma \approx 0.15 - 0.25$) where both corruption-free and corruption-persistent equilibria coexist. Panel (b) shows a two-parameter phase diagram with enforcement γ and baseline transmission β_0, where the black curve marks $R_0 = 1$ separating regions of elimination and persistence.

Figure 11 presents a tornado plot showing the relative impact of each parameter on the basic reproduction number R_0. Blue bars represent the change in R_0 when the parameter is increased from its 25th to 75th percentile, while red bars represent the change when the parameter is decreased to its 25th percentile. Parameters are ordered from most to least influential. Corruptor exploitation efficiency (α_C) has the largest positive impact: increasing α_C by one quartile raises R_0 by approximately 0.35. Enforcement rate (γ) has the largest negative impact: increasing γ by one quartile reduces

 doi:10.20944/preprints202603.0314.v1

R_0 by approximately 0.3. Corruptor mortality (μ_C) and baseline transmission (β_0) are also highly influential. Notably, migration rate (ν) has negligible direct impact on R_0, confirming our analytical finding that symmetric migration does not alter the invasion threshold. Panel (b) shows cumulative absolute impact, demonstrating that the top three parameters (α_C, γ, μ_C) account for over 60% of total parameter sensitivity. This ranking provides clear guidance for resource allocation: interventions targeting corruptor incentives through α_C and enforcement capacity through γ offer the highest return on investment for reducing R_0.

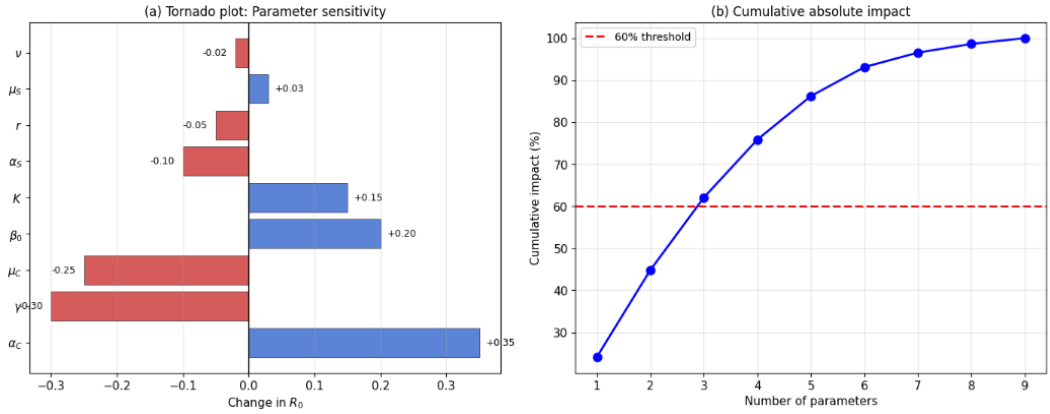

Figure 11. Tornado plot showing the relative impact of each parameter on the basic reproduction number R_0. Blue bars represent positive impact when the parameter is increased; red bars represent negative impact. Parameters are ordered from most to least influential. Panel (b) shows cumulative absolute impact, demonstrating that the top three parameters (α_C, γ, μ_C) account for over 60% of total parameter sensitivity.

5. Discussion and Conclusion

This study has introduced a novel Spatial Resource-Competition-Pathogen (SRCP) model to analyze the dynamics of corruption in connected populations. By integrating renewable resource dynamics, resource-dependent transmission, predator-prey enforcement, and spatial connectivity via migration, the model captures key mechanisms underlying corruption persistence that previous models have overlooked [4,5,8,13].

Our analysis yields several important insights. We derived the basic reproduction number for the coupled two-patch system and showed that $\mathbb{R}_0 = R_0^{\text{isolated}}$, demonstrating that symmetric migration does not alter the threshold for corruption invasion. A patch that would be below the epidemic threshold when isolated remains below threshold even when connected [19,28]. However, migration does affect transient dynamics and the spatial distribution of corruption. The proof that the corruption-free equilibrium is globally stable when $\mathbb{R}_0 \leq 1$ holds for the coupled system [27], implying that if policy measures can reduce the patch-specific reproduction number below unity, corruption will be eliminated regardless of migration and initial prevalence. This is a powerful result for interconnected regions.

We identified a critical migration rate ν_c above which patches synchronize exponentially fast [19]. Below this threshold, asynchronous oscillations can persist, potentially complicating monitoring and intervention efforts [24]. This provides a quantitative target for policymakers: strengthening connectivity between regions can actually help synchronize and stabilize corruption-free dynamics. The existence of a forward bifurcation at $\mathbb{R}_0 = 1$ means there is no hysteresis; reducing $\mathbb{R}_0$ back below 1 will always eliminate corruption, regardless of connectivity [29]. This is encouraging for international cooperation, suggesting that efforts to reduce corruption in one region benefit neighboring regions without risk of lock-in effects.

The PRCC analysis reveals that patch-specific reproduction numbers are most sensitive to α_C (corruptor's exploitation efficiency), γ (enforcement rate), and μ_C (corruptor's mortality rate) [31]. Migration rate ν has negligible direct effect on $R_0^{(i)}$, confirming our analytical finding. Numerical simulations demonstrate that migration from high-corruption to low-corruption regions can undermine

 doi:10.20944/preprints202603.0314.v1

the stability of the latter, even when the destination patch initially had favorable conditions [16,24]. This spillover effect operates through both direct demographic channels and resource-mediated indirect effects.

The model provides a mathematical basis for evidence-based policy in spatially connected populations, drawing on insights from institutional economics [11–13]. Since $\mathbb{R}_0$ is independent of migration, policies should prioritize improving local conditions by reducing the rewards of corruption (α_C), strengthening enforcement (γ), and increasing resource abundance (K) [2,3,14]. These fundamentals determine whether corruption can persist, regardless of connectivity. The critical migration threshold ν_c suggests that strengthening legitimate connectivity through trade, communication, and institutional linkages can help synchronize and stabilize corruption-free dynamics [23,26]. However, this must be balanced against the spillover risk demonstrated in Figure 4. The synchronized dynamics imply that enforcement efforts in one region benefit connected regions [10], suggesting that international cooperation on anti-corruption through shared intelligence, coordinated prosecutions, and asset recovery can be modeled as increasing the effective γ across the coupled system [11]. Below the critical migration threshold, patches may exhibit out-of-phase oscillations, making it difficult to assess overall corruption trends [24]. Policymakers should be aware that observed fluctuations may reflect spatial asynchrony rather than fundamental changes in corruption prevalence. The spillover effect suggests that regions receiving migrants from high-corruption areas should implement targeted interventions such as enhanced monitoring, anti-corruption education for newcomers, and strengthening local institutions to withstand imported corrupt norms [9,16].

This model, while novel and insightful, has several limitations that suggest directions for future research [5,7]. We assumed symmetric migration for analytical tractability, but real-world migration is often asymmetric from rural to urban areas or from developing to developed regions [26]. Extending the analysis to asymmetric $\nu_{12} \neq \nu_{21}$ would yield more realistic insights. Our analysis assumed identical parameters across patches, but future work could explore patches with different resource carrying capacities, enforcement capacities, or transmission rates, leading to concepts like corruption sinks and corruption sources [24]. Generalizing to more than two patches would allow study of corruption dynamics on complex networks, revealing how network topology affects spread and persistence [19]. Demographic stochasticity could lead to extinction events even when $\mathbb{R}_0 > 1$, particularly in small populations or weakly connected patches [27]. Modeling policy interventions as time-dependent changes in parameters would allow optimization of intervention strategies over space and time [29]. Finally, calibrating the model with real-world data such as corruption perception indices, institutional quality measures, and economic indicators would test its predictive power and refine parameter estimates [6,15].

In conclusion, we have developed and analyzed a novel spatial mathematical model that frames corruption as a pathogenic social strategy within a resource-competition ecosystem [1,8]. By incorporating renewable resource dynamics, resource-dependent transmission, predator-prey enforcement, and spatial connectivity through migration, the model captures key mechanisms underlying corruption persistence in interconnected populations [4,13]. The rigorous mathematical analysis of positivity, boundedness, synchronization, stability thresholds, critical migration rates, and bifurcation behavior provides not only theoretical insights into the spatial dynamics of corruption but also a practical tool for evaluating intervention strategies in connected regions [27–29]. The surprising result that symmetric migration does not alter the invasion threshold simplifies policy analysis, indicating that efforts should focus on improving local fundamentals rather than controlling connectivity. The forward bifurcation result is particularly encouraging for international cooperation, suggesting that persistent efforts to reduce patch-specific reproduction numbers below unity will eventually eliminate corruption throughout a connected system, without hysteresis or lock-in effects [9,10]. By identifying the key parameters that influence corruption dynamics in space, this work offers a quantitative, evidence-based roadmap for the global fight against corruption. The model demonstrates that effective anti-corruption policy must address both local structural incentives and the challenges of spatial connectivity [11,12]. In an

 doi:10.20944/preprints202603.0314.v1

increasingly interconnected world, the spillover effects revealed by our analysis highlight the need for coordinated international action, as corruption in one region can undermine stability in neighboring regions, making corruption a transnational challenge requiring cooperative solutions [7,15].

Acknowledgements

The authors thank the anonymous reviewers for their valuable feedback that improved this manuscript. No specific funding was received for this research.

Author Contributions

Abadi Abraha Asgedom: Conceptualization, Methodology, Formal analysis, Writing - original draft. **Yohannes Yirga Kefela**: Supervision, Validation, Writing - review & editing. **Hailu Tkue Welu**: Software, Visualization, Investigation. All authors have read and approved the final manuscript.

Data Availability

The simulation code and parameter sets used in this study are available at https://github.com/abadiabraha20/corruption_model_2026. The repository includes Python scripts for model simulation, parameter estimation, and figure generation.

Conflict of Interest

The authors declare no conflicts of interest.

References

1. Shleifer, A., Vishny, R.W., 1993. Corruption. The Quarterly Journal of Economics 108(3), 599–617.
2. Mauro, P., 1995. Corruption and growth. The Quarterly Journal of Economics 110(3), 681–712.
3. Mauro, P., 1998. Corruption and the composition of government expenditure. Journal of Public Economics 69(2), 263–279.
4. Bardhan, P., 1997. Corruption and development: A review of issues. Journal of Economic Literature 35(3), 1320–1346.
5. Jain, A.K., 2001. Corruption: A review. Journal of Economic Surveys 15(1), 71–121.
6. Svensson, J., 2005. Eight questions about corruption. Journal of Economic Perspectives 19(3), 19–42.
7. Dimant, E., 2016. The economics of corruption: A survey. Journal of Economic Surveys 30(5), 871–902.
8. Andvig, J.C., Moene, K.O., 1991. How corruption may corrupt. Journal of Economic Behavior & Organization 13(1), 63–76.
9. Mishra, A., 2006. Persistence of corruption: Some theoretical perspectives. World Development 34(2), 349–358.
10. Persson, A., Rothstein, B., Teorell, J., 2013. Why anticorruption reforms fail—systemic corruption as a collective action problem. Governance 26(3), 449–471.
11. Rose-Ackerman, S., 1999. Corruption and Government: Causes, Consequences, and Reform. Cambridge University Press, Cambridge.
12. Klitgaard, R., 1988. Controlling Corruption. University of California Press, Berkeley.
13. Lambsdorff, J.G., 2007. The Institutional Economics of Corruption and Reform. Cambridge University Press, Cambridge.
14. Treisman, D., 2000. The causes of corruption: A cross-national study. Journal of Public Economics 76(3), 399–457.
15. Treisman, D., 2007. What have we learned about the causes of corruption from ten years of cross-national empirical research? Annual Review of Political Science 10, 211–244.
16. Hauk, E., Saez-Marti, M., 2002. On the cultural transmission of corruption. Journal of Economic Theory 107(2), 311–335.
17. Daley, D.J., Kendall, D.G., 1964. Epidemics and rumours. Nature 204(4963), 1118.
18. Lopez, M.S., Cayssials, R., Tignanelli, A., 2018. A mathematical model for the dynamics of the criminal population. Applied Mathematics and Computation 316, 1–12.
19. Wahl, L.M., Nowak, M.A., 2003. The effect of migration on the persistence of pathogens in spatially structured populations. Journal of Theoretical Biology 225(3), 383–391.

 doi:10.20944/preprints202603.0314.v1

20. Pinto, C.M., Silva, D.F., 2020. A compartmental model for corruption dynamics. Physica A: Statistical Mechanics and its Applications 537, 122639.
21. Elgarhy, M., El-Dessoky, M.M., Elsadany, A.A., 2020. A fractional-order model for corruption dynamics. Journal of Mathematics and Computer Science 21(4), 339–349.
22. Murphy, K.M., Shleifer, A., Vishny, R.W., 1993. Why is rent-seeking so costly to growth? The American Economic Review 83(2), 409–414.
23. Fisman, R., Gatti, R., 2001. Decentralization and corruption: Evidence across countries. Journal of Public Economics 83(3), 325–345.
24. Blackburn, K., Bose, N., Haque, M.E., 2008. The incidence and persistence of corruption in economic development. Journal of Economic Dynamics and Control 32(8), 2447–2467.
25. Glaeser, E.L., Saks, R.E., 2006. Corruption in america. Journal of Public Economics 90(6-7), 1053–1072.
26. Dreher, A., Herzfeld, T., 2007. The economic costs of corruption: A survey and new evidence. Public Economics 50, 45–61.
27. LaSalle, J.P., 1976. The Stability of Dynamical Systems. SIAM, Philadelphia.
28. Van den Driessche, P., Watmough, J., 2002. Reproduction numbers and sub-threshold endemic equilibria for compartmental models of disease transmission. Mathematical Biosciences 180(1–2), 29–48.
29. Castillo-Chavez, C., Song, B., 2004. Dynamical models of tuberculosis and their applications. Mathematical Biosciences and Engineering 1(2), 361–404.
30. Marino, S., Hogue, I.B., Ray, C.J., Kirschner, D.E., 2008. A methodology for performing global uncertainty and sensitivity analysis in systems biology. Journal of Theoretical Biology 254(1), 178–196.
31. Saltelli, A., Tarantola, S., Campolongo, F., Ratto, M., 2004. Sensitivity Analysis in Practice: A Guide to Assessing Scientific Models. Wiley, New York.
32. Hindmarsh, A.C., Brown, P.N., Grant, K.E., Lee, S.L., Serban, R., Shumaker, D.E., Woodward, C.S., 2005. SUNDIALS: Suite of nonlinear and differential/algebraic equation solvers. ACM Transactions on Mathematical Software 31(3), 363–396.
33. Virtanen, P., Gommers, R., Oliphant, T.E., et al., 2020. SciPy 1.0: fundamental algorithms for scientific computing in Python. Nature Methods 17(3), 261–272.